BSC

Model Administrative Change Notice

Complete only applicable items.

1. Document Number:	MDL-NBS-HS-000017	2. Revision:	01	3. ACN:	01
4. Title:	DRIFT SCALE THM MODEL				
5. No. of Pages Attached	21				

6. Approvals:

Preparer:	Wendy Mitcheltree (Print name and sign) Wendy Mitcheltree	12-15-05 (Date)
Checker:	Bruce Kirstein (Print name and sign) Bruce E. Kirstein	12-15-05 (Date)
QER:	Darrell Svalstad (Print name and sign) Darrell K Svalstad	12-16-05 (Date)
Independent Technical Reviewer:	Rob Howard (Print name and sign) RWH for Rob Howard	12/20/05 (Date)
Responsible Manager:	Ernest Hardin (Print name and sign) E Hardin	1/3/06 (Date)

7. Affected Pages	8. Description of Change:
1-1	Citation changed (DIRS updated as appropriate) Replace citation, change: *Scale Coupled Processes (DST and TH Seepages) Models* (BSC 2004 [DIRS 170338], Appendix B). to DTN: LL000114004242.090 [DIRS 142884] (file: *TSPA_SR_mean_disk1.tar, chimney_infiltration_fluxes*) Part of the resolution of CR-5600.
4-2	Citation changed (DIRS updated as appropriate) Replace citation, change: Figure 7-21 in *Drift Degradation Analysis* (BSC 2004 [DIRS 166107]), to be consistent with that report. to the figure in DTN: MO0408MWDDDMIO.002 [DIRS 171483] (file: *MO0408MWDDDMIO_002RPC1.zip, summary10MPa03seed5.xls*, sheet "envelope-c") Part of the resolution of CR-5600.

1. Document Number:	MDL-NBS-HS-000017	2. Revision:	01	3. ACN:	01
4. Title:	DRIFT SCALE THM MODEL				

4-6	Citation changed (DIRS updated as appropriate) Replace citation, change: (BSC 2004 [DIRS 169856], Tables 6.5-2 and 6.7-2). to (BSC 2005 [DIRS 172862], Table 6.5-2). Part of the resolution of TBV-6328.
4-12	Citation changed (DIRS updated as appropriate) Replace citation in Table 4.1-1a, change: BSC 2004 DIRS [166107] Figure 7-21 to DTN: MO0408MWDDDMIO.002 [DIRS 171483], file: *MO0408MWDDDMIO_002RPC1.zip, summary10MPa03seed5.xls, sheet "envelope-c"* Part of the resolution of CR-5600.
4-12	Citation changed (DIRS updated as appropriate) Replace citation Table 4.1-1a change: BSC 2004 [DIRS 170338], Appendix B to DTN:LL000114004242.090 [DIRS 142884], file: *TSPA_SR_mean_disk1.tar, chimney_infiltration_fluxes* Part of the resolution of CR-5600.
4-14, 6-31, and 6-53	Citation changed (DIRS updated as appropriate) Update citation in Table 4.1-1b on 4-14 , 6-31, and 6-53 change: BSC 2004 [DIRS 170004], 6.1.2-12 to 6.1.2-16 to BSC 2004 [DIRS 170004], 6-19 to 6-23 Part of the resolution of TBV-6315.

1. Document Number:	MDL-NBS-HS-000017	2. Revision:	01	3. ACN:	01
4. Title:	DRIFT SCALE THM MODEL				

4-17 and 7-40	Citation changed (DIRS updated as appropriate) Replace citation, in Table 4.1-3b and Table 7.6-1change: BSC 2004 [DIRS 166107], Figure 7-21 to DTN: MO0408MWDDDMIO.002 [DIRS 171483], file: *MO0408MWDDDMIO_002RPC1.zip, summary10MPa03seed5.xls, sheet "envelope-c"* Part of the resolution of CR-5600.
6-18	Citation changed (DIRS updated as appropriate) Replace citation, change: *Drift Scale Coupled Processes (DST and THC Seepage) Models* (BSC 2004 [DIRS 169856], Sections 6.5 and 6.7). to *Drift-Scale THC Seepage Model* (BSC 2005 [DIRS 172862], Section 6.5). Part of the resolution of TBV-6328.
6-19	Added citation (DIRS updated as appropriate) Added citation: , and presented in DTN: LL000114004242.090 [DIRS 142884] (file: *TSPA_SR_mean_disk1.tar, chimney_infiltration_fluxes*). Part of the resolution of CR-5600.
6-23	Citation changed (DIRS updated as appropriate) Replace citation, change: (BSC 2004 [DIRS 169856], Sections 6.5 and 6.7). to (BSC 2005 [DIRS 172862], Section 6.5). Part of the resolution of TBV-6328.

1. Document Number:	MDL-NBS-HS-000017	**2. Revision**:	01	**3. ACN:**	01
4. Title:	DRIFT SCALE THM MODEL				

6-35, 6-80, and 6-83	Citation changed (DIRS updated as appropriate) Update citation, change: BSC 2004 [DIRS 170004], Table 6.1.2-1 to BSC 2004 [DIRS 170004] Table 6-2 Part of the resolution of TBV-6315.
7-40	Citation changed (DIRS updated as appropriate) Replace citation, in Table7.6-1 NOTE change: Figure 7-21 in *Drift Degradation Analysis* (BSC 2004 [DIRS 166107]) to the figure in DTN: MO0408MWDDDMIO.002 [DIRS 171483] (file: *MO0408MWDDDMIO_002RPC1.zip, summary10MPa03seed5.xls, sheet "envelope-c")* Part of the resolution of CR-5600.
9-3	Citation changed: Replace citation, change: BSC 2004. *Drift-Scale THC Seepage Model.* MDL-NBS-HS-000001 REV 03. Las Vegas, Nevada: Bechtel SAIC Company. 169856 to BSC 2005. *Drift-Scale THC Seepage Model.* MDL-NBS-HS-000001 REV 04,. Las Vegas, Nevada: Bechtel SAIC Company. ACC: DOC.20050218.0001. 172862 Part of the resolution of TBV-6328.

1. PURPOSE

This model report documents the drift scale coupled thermal-hydrological-mechanical (THM) processes model development and presents simulations of the THM behavior in fractured rock close to emplacement drifts. The modeling and analyses are used to evaluate the impact of THM processes on permeability and flow in the near-field of the emplacement drifts. The results from this report are used to assess the importance of THM processes on seepage and support in the model reports *Seepage Model for PA Including Drift Collapse* and *Abstraction of Drift Seepage*, and to support arguments for exclusion of features, events, and processes (FEPs) in the analysis reports *Features, Events, and Processes in Unsaturated Zone Flow and Transport* and *Features, Events, and Processes: Disruptive Events*. The total system performance assessment (TSPA) calculations do not use any output from this report.

Specifically, the coupled THM process model is applied to simulate the impact of THM processes on hydrologic properties (permeability and capillary strength) and flow in the near-field rock around a heat-releasing emplacement drift. The heat generated by the decay of radioactive waste results in elevated rock temperatures for thousands of years after waste emplacement. Depending on the thermal load, these temperatures are high enough to cause boiling conditions in the rock, resulting in water redistribution and altered flow paths. These temperatures will also cause thermal expansion of the rock, with the potential of opening or closing fractures and thus changing fracture permeability in the near-field. Understanding the THM coupled processes is important for the performance of the repository because the thermally induced permeability changes potentially effect the magnitude and spatial distribution of percolation flux in the vicinity of the drift, and hence the seepage of water into the drift. This is important because a sufficient amount of water must be available within a drift to transport any exposed radionuclides out of the drift to the groundwater below, and eventually to people within the accessible environment. Absent sufficient water, radionuclides cannot be transported and there would be no significant health effect on people, even if radioactive waste containers were damaged or corroded to such an extent that radionuclides were exposed to water.

Inputs from other project reports to this model report include repository drift configuration, thermal line load, ventilation efficiency, infiltration rates and certain mechanical rock properties. The thermal line load of 1.45 kW/m and 50-year ventilation period used in this model report are described in the repository design drawing, *D&E/ PA/C IED Emplacement Drift Configuration and Environment* (BSC 2004 [DIRS 168489], effective date 3/26/2004). Time-dependent thermal-line-load values stem from the repository design drawing, *Repository Design, Repository/PA IED Subsurface Facilities Plan Sht. 5 of 5* (BSC 2002 [DIRS 159527], effective date 05/20/2002), and the ventilation efficiency of 86.3 percent is taken from *Ventilation Analysis and Model Report* (BSC 2002 [DIRS 160975], Table 6-6). Mean infiltration rates were taken from DTN: LL000114004242.090 [DIRS 142884] (file: *TSPA_SR_mean_disk1.tar*, chimney_infiltration_fluxes). In addition, certain rock mechanical properties were taken from the recent *Drift Degradation Analysis* (BSC 2004 [DIRS 166107], Table E-10).

The main model outputs from this model report are the potential changes in key hydrologic properties (permeability and capillary strength). In addition, the impact of THM coupling on the

flow field around the drift is assessed. The results supplement thermal seepage results from thermal-hydrological (TH) simulations reported in the model report entitled *Drift-Scale Coupled*

[DIRS 168481] only apply to rock units located away from the repository. A detailed comparison of the thermal properties of the two sets provided in Table C-1 of *Drift-Scale Coupled Processes (DST and TH Seepage) Models* (BSC 2004 [DIRS 170338]) shows that the differences are generally within a few percent but is substantial for some of the units. The largest difference occurs in the tsw31 unit where revised bulk thermal conductivity is about 40 percent higher in the revised data. However, a sensitivity analysis documented in Appendix D of this model report shows that these differences in thermal properties do not significantly impact the results and conclusions presented in this model report, which addresses the effects in the near-field rock. Although a 40 percent increase in thermal conductivity in tsw31 may appear significant, it is not because the tsw31 layer is located more than 100 meters away from the emplacement drift where there is small effect from the repository thermal load. In addition, this layer is only a few meters thick (see Table 4.1-3c for location and thickness).

The basic mechanical properties of the rock mass (Young's Modulus and Poisson's ratio) are developed using an established engineering geological rock mass quality classification system with associated empirical relationships (Section 6.4.2). These properties are derived within this model report from qualified sources of laboratory measurements and field mapping in the Exploratory Studies Facility (ESF). The properties are derived (from the qualified input sources) in a Microsoft Excel spreadsheet: THM rock mass modulus v1.xls, which has been submitted to the Technical Data Management System (TDMS) under output DTN: LB0306DRSCLTHM.001. For a base case of mechanical properties, the Young's modulus and Poisson's ratio for TCw, PTn, TSw1, and TSw2 TM units are developed in: THM rock mass modulus v1.xls. The mechanical properties of TSw3 are assumed to be equal to TSw2 (see Assumption 3 in Section 5), and the mechanical properties of the CHn TM unit are extracted from mean of intact rock values extracted from DTN: SNL02030193001.026 [DIRS 108436], Table S99119_002 (see Assumption 4 in Section 5). For a sensitivity case of a low quality lithophysal rock—rocks with a high percentage of lithophysal porosity with relatively low bulk and shear modulus, and relatively low rock strength—the mechanical properties of the Tptpll unit is extracted from properties developed in the recent *Drift Degradation Analysis* (BSC 2004 [DIRS 166107], Table E-10, Category 1). Further justification for the adopted mechanical properties is given in Section 6.4.2.

Source DTNs and references for hydrological, thermal, and mechanical properties are given in Tables 4.1-1a and b. For quick reference, values of these properties are listed in Tables 4.1-3a and b for the Topopah Spring Tuff middle nonlithophysal (Tptpmn or tsw34) and lower lithophysal (Tptpll or tsw35) stratigraphic units, in which the main part of the repository will be located. For the sake of completeness, properties for the upper lithophysal (Tptpul or tsw33) unit are also provided. The values for the low quality lithophysal properties, which are used in the above mentioned sensitivity study, are listed in Table 4.1-3b. The tensile strength of 0.8 Mpa, given in Table 4.1-3b, was obtained from the x-intercept of the figure in DTN: MO0408MWDDDMIO.002 [DIRS 171483] (file: *MO0408MWDDDMIO_002RPC1.zip*, *summary10MPa03seed5.xls*, sheet "envelope-c").

In addition, properties for the rock mass stress-permeability relationship and rock mass thermal expansion coefficient are developed within this model report according to

Sections 6.4.3 and 6.4.4. Source DTNs and references used for developing those data are given in Table 4.1-1b. The rock mass thermal expansion coefficient is derived from laboratory data in

(BSC 2005 [DIRS 172862], Table 6.5-2). The specific values used in this model report are presented in Tables 4.1-3e and 6.3-1, and Figure 6.3-1. Source DTNs for hydraulic and thermal boundary conditions are given in Table 4.1-1a.

The mechanical boundary conditions are zero displacement restrictions on displacements normal to the bottom and the lateral (vertical side of the model) boundaries and the top of the model (ground surface) is free to move. Thus, there are no data sources needed for mechanical boundary conditions. The mechanical boundary conditions are justified in Section 6.3.

Initial stress (before excavation) for all the model domains of the drift scale THM model is estimated according to Assumption 2, Section 5, using sources of saturated density given in Table 4.1-1b.

4.1.1.3 Thermal Load

The thermal output of individual waste packages placed into drifts is represented by an average thermal line load, which is 1.45 kW/m according to current designs. A 50-year ventilation period is considered, in which a significant fraction of the heat is removed from the repository. The thermal line load of 1.45 kW/m and 50-year ventilation period are described in repository-design drawing, *D&E/ PA/C IED Emplacement Drift Configuration and Environment* (BSC 2004 [DIRS 168489], effective date 3/26/2004). Note that the value of 1.45 kW/m refers to the initial thermal line load at emplacement time. This value decreases with time as a result of radioactive decay. The time-dependent thermal-line-load values used in this report stems from the repository design drawing, *Repository Design, Repository/PA IED Subsurface Facilities Plan Sht. 5 of 5* (BSC 2002 [DIRS 159527], effective date 05/20/2002). More recent time-dependent thermal-line-load values are available in the repository design drawing *D&E/PA/C IED Typical Waste Package Components Assembly* (BSC 2004 [DIRS 167369], effective date 01/30/2004). The time-dependent thermal-line-load values are virtually identical in the two sources, and hence no impact is expected on the TH simulations in this model report.

Ventilation efficiency denotes the fraction of heat removed from the repository as a result of ventilation during the 50-year preclosure period. The ventilation efficiency is time-dependent and average values of the integrated ventilation efficiency are used for simplification. The integrated ventilation efficiency provided by current Yucca Mountain Project (YMP) reports is 88 percent (DTN: MO0306MWDASLCV.001 2003 [DIRS 165695]) when the emplacement drift is 600 m in length. When the emplacement drift is 800-m long, integrated ventilation efficiency is calculated to be 86 percent (DTN: MO0307MWDAC8MV.000 2003 [DIRS 165395]). Further details on the calculation of these ventilation efficiencies are provided in *Ventilation Analysis and Model Report* (BSC 2004 [DIRS 169862], Equation 6-6). Uncertainties in calculated integrated ventilation efficiencies have also been addressed (BSC 2004 [DIRS 169862], Section 8.2.1). For both 600 m and 800 m long drifts, the standard deviation of the calculated ventilation efficiency is 3 percent (BSC 2004 [DIRS 169862], Table 8-2). Thus, the ventilation efficiency can be in the range 85 to 91 percent for a 600 m long drift. For 800 m long drifts, the range of ventilation efficiency is 83 to 89 percent.

The ventilation efficiency value used in this model report is 86.3 percent. The 86.3 percent value was reported in an earlier version of *Ventilation Analysis and Model Report* (BSC 2002

4.1.3.3 Displacement Measurements at DST

Displacement data have been continuously collected from multiple-point borehole extensometers (MPBX) at the DST. For model validation, these measured displacements are directly compared against simulated displacements from the model simulation. The DTN for the measured displacement data is given in Table 4.1-5.

4.1.3.4 Air-Permeability Measurements at Niches

Air-permeability measurements were conducted at several excavated niches to study permeability changes near a drift wall caused by excavation effects (i.e., mechanical unloading of the rock mass near the drift wall, causing fracture opening and consequently permeability increase). These types of tests were conducted at three excavated niches located in the Tptpmn unit and one excavated niche located in the Tptpll unit (BSC 2004 [DIRS 170004], Section 6.1). For model validation, the measured changes in permeability induced by the excavation of the niches (air-permeability ratio) are compared to model simulations. The DTN for measured air-permeability ratios is given in Table 4.1-5.

Table 4.1-1a. Data Tracking Numbers for Sources of Data Input to the Drift Scale THM Model Used for Predictive Analysis

DTN/Reference	Description	TDMS Input	Design Input	Other Analyses
Rock Properties (Section 4.1.1.1)				
LB0205REVUZPRP.001 [DIRS 159525]	Fracture porosity, frequency, and surface area (Table 4.1-3a)	X		
LB0208UZDSCPMI.002 [DIRS 161243]	Fracture and matrix calibrated parameters—mean infiltration (Table 4.1-3a)	X		
LB0210THRMLPRP.001 [DIRS 160799][1]	Matrix thermal data and porosity	X		
BSC 2004 [DIRS 166107], Table E-10, Category 1, and DTN: MO0408MWDDDMIO.002 [DIRS 171483], file: *MO0408MWDDDMIO_002RPC1.zip, summary10MPa03seed5.xls*, sheet "envelope-c"	Rock mass mechanical properties for low quality lithophysal rock in Tptpll (Table 4.1-3b, Section 6.7)			X
Boundary Conditions (Section 4.1.1.2)				
DTN: LL000114004242.090 [DIRS 142884], file: *TSPA_SR_mean_disk1.tar*, chimney_infiltration_fluxes	Infiltration rates for present day, monsoon, and glacial periods (Table 6.3-1 and Figure 6.3-1). The median infiltration case is used in this report for both Tptpmn and Tptpll model domains.			X

LB991131233129.004 [DIRS 162183] File “pa99cal_ecm.out” : Elements Tpi64 and Bti64 for top and bottom of Tptpmn model domain Elements Tpj34 and Btj34 for top and bottom of Tptpll model domain	Top and bottom boundary temperatures, pressure, liquid/gas saturations (Table 6.3-1 and Figure 6.3-1). At borehole USW SD-9 for Tptpmn model domain (Nevada State Plane coord. E171234, N234074). At center of the repository for Tptpll model domain (Nevada State Plane coord. E170572, N233195).	X		

Table 4.1-1b. Data Tracking Numbers for Sources for Data Developed or Estimated in this Model Report Used as Input to the Drift Scale THM Model for Predictive Analysis (Continued)

DTN/Reference	Description	TDMS Input	Design Input	Other Analyses
Rock Properties (Section 4.1.1.1) (Continued)				
SNL02030193001.020 [DIRS 108432] SNL02030193001.021 [DIRS 108433] SNL02030193001.022 [DIRS 109613] SNL02030193001.023 [DIRS 108435] SNL02030193001.024 [DIRS 122530] SNL02030193001.026 [DIRS 108436]	Intact rock properties from laboratory tests for development of rock mass mechanical properties (Young's modulus and Poisson's ratio in Table 4.1-3a) using Excel spreadsheet entitled *THM rock mass modulus v1.xls* (Section 6.4.2; Section 5, Assumptions 3 and 4).	X		
GS950508314224.003 [DIRS 107488] GS960908314224.020 [DIRS 106059] GS000608314224.006 [DIRS 152572] GS960908314224.015 [DIRS 108372] GS960908314224.016 [DIRS 108373] GS960908314224.017 [DIRS 108376] GS970108314224.002 [DIRS 107490] GS970208314224.004 [DIRS 107492] GS970808314224.009 [DIRS 107494] GS970808314224.011 [DIRS 107495] GS970808314224.013 [DIRS 107497]	Field mapping of rock quality parameters along ESF for development of rock mass mechanical properties (Young's modulus and Poisson's ratio in Table 4.1-3a) using Excel spreadsheet entitled *THM rock mass modulus v1.xls* (Section 6.4.2; Section 5, Assumptions 3 and 4). Note that this table only lists ESF data since only ESF data was used to derive the adopted rock mass properties. *THM rock mass modulus V1.xls* lists sources from both ESF and ECRB Cross Drift used for comparison.	X		
LB970600123142.001 [DIRS 105589] LB980120123142.004 [DIRS 105590] LB980120123142.005 [DIRS 114134], with calculated mean value documented in BSC (2004 [DIRS 170038]), Figure 6-2.	Fracture permeability of Tptpmn unit around the DST for development of a rock mass stress-permeability relationship (Section 6.4.4, Figure 6.4.4-2, Appendix A).	X		
LB0205REVUZPRP.001 [DIRS 159525]	Fracture frequency of the Tptpmn unit for development of a rock mass stress-permeability relationship (Section 6.4.4, Appendix A).	X		
LB0208AIRKDSTH.001 [DIRS 160897]	Permeability change factor at the DST used for development of a rock mass stress-permeability relationship (Section 6.4.4, Figure 6.4.4-2, Appendix A).	X		
LB0310AIRK0015.001 [DIRS 168564], BSC (2004 [DIRS 170004], Figures 6-19 to 6-23).	Pre to post excavation permeability ratio at Niche Tests used for development of a rock mass stress-permeability relationship (Section 6.4.4, Figure 6.4.4-2, Appendix A).	X		
SNL01B05059301.006 [DIRS 129168], with calculation of mean values documented in Brodsky et al. (1997 [DIRS 100653], Table 4-4).	Laboratory thermal expansion coefficient for development of a temperature dependent thermal expansion coefficient (Section 6.4.3, Figure 6.4.3-1).	X		

Table 4.1-3a. Summary of Rock Properties of Geologic Units Tptpul, Tptpmn, and Tptpll in the Drift Scale THM Model Applied to the Tptpll and Tptpmn Model Domains for Predictive Analysis (Continued)

Geologic Framework Model Unit >		Tptpul	Tptpmn	Tptpll	Source
Fracture Hydrological Properties					
Hydrogeological Unit > (Label for fracture properties)>		**TSw33 (TswF3)**	**TSw34 (TswF4)**	**TSw35 (TswF5)**	
Permeability	k_f (m^2)	7.80E-13	3.30E-13	9.10E-13	LB0205REVUZPRP.001 [DIRS 159525]
Porosity	f_f (-)	5.8E-3	8.5E-3	9.6E-3	LB0208UZDSCPMI.002 [DIRS 161243]
Van Genuchten α	α_f (1/Pa)	1.59E-3	1.04E-4	1.02E-4	LB0208UZDSCPMI.002 [DIRS 161243]
Van Genuchten m (or λ)	m_f (-)	0.633	0.633	0.633	LB0208UZDSCPMI.002 [DIRS 161243]
Residual saturation	S_{lrf} (-)	0.01	0.01	0.01	LB0208UZDSCPMI.002 [DIRS 161243]
Fracture frequency	f (m^{-1})	0.81	4.32	3.16	LB0205REVUZPRP.001 [DIRS 159525]
Fracture surface area	A_f (m^2/m^3)	4.44	13.54	9.68	LB0205REVUZPRP.001 [DIRS 159525]
Active fracture coefficient	γ (-)	0.600	0.569	0.569	LB0208UZDSCPMI.002 [DIRS 161243]
Rock Mass Mechanical Properties					
Thermal Mechanical Unit >		**TSw1**	**TSw2**	**TSw2**	
Young's Modulus	E (GPa)	19.40[1]	14.77[1]	14.77[1]	These properties were derived in Excel spreadsheet entitled *THM rock mass modulus v1.xls* from the qualified sources listed in Table 4.1-1b under items about intact rock properties and field mapping.
Poisson's Ratio	ν (-)	0.23[1]	0.21[1]	0.21[1]	

[1] The listed values can be found in the Microsoft Excel spreadsheet entitled *THM rock mass modulus v1.xls* in output DTN: LB0306DRSCLTHM.001.

Table 4.1-3b. Low Quality Lithophysal Rock Properties Applied to the Tptpll Model Domain as a Sensitivity Case of Predictive Analysis

Property		Value	Source
Young's Modulus	E (GPa)	1.9	BSC 2004 [DIRS 166107], Table E-10, Category 1
Bulk Modulus	K (GPa)	1.07	BSC 2004 [DIRS 166107], Table E-10, Category 1
Shear Modulus	G (GPa)	0.8	BSC 2004 [DIRS 166107], Table E-10, Category 1
Cohesion for ϕ = 40°	C (MPa)	2.33	BSC 2004 [DIRS 166107], Table E-10, Category 1
Tensile Strength	T (MPa)	0.8	DTN: MO0408MWDDDMIO.002 [DIRS 171483], file: *MO0408MWDDDMIO_002RPC1.zip, summary10MPa03seed5.xls*, sheet "envelope-c"

6.3 TPTPMN AND TPTPLL MODEL DOMAINS

The drift scale THM model is a two-dimensional model that extends from the ground surface down to the groundwater table. It includes one-half of the emplacement drift as a result of lateral symmetry (Figure 6.3-1a). Coupled THM simulations were conducted on two model domains, representing two different vertical two-dimensional cross sections through the interior of the repository at Yucca Mountain. The first one, the Tptpmn model domain, considers a waste emplacement drift located in the Topopah Spring Tuff middle nonlithophysal unit (Tptpmn unit). The second one, the Tptpll model domain, has a drift located in the Topopah Spring lower lithophysal unit (Tptpll unit). The two sections are selected to account for the two main host rock units of the repository and are the same sections being considered in both the *Drift-Scale Coupled Processes (DST and TH Seepage) Models* report (BSC 2004 [DIRS 170338], Section 6.2) and *Drift-Scale THC Seepage Model* (BSC 2005 [DIRS 172862], Section 6.5). TOUGH2 dual-permeability meshes of both the Tptpmn and Tptpll model domains were constructed using the qualified software 2KGRIDV1.F V1.0 (STN: 10244-1.0-00; LBNL 2000 [DIRS 147553]). As mentioned in Section 6.2.1, in the repository units, three major sets of fractures are oriented almost orthogonal to each other (CRWMS M&O 1998 [DIRS 102679], Section 7.4.5; BSC 2004 [DIRS 166107], Section 6.1.4.1), two subvertical and one subhorizontal. More specifically, in the TSw2 TM unit, these major fracture sets (Tptpmn unit) are (CRWMS M&O 1998 [DIRS 102679], Section 7.4.5):

1. One prominent vertical, southeast trending
2. One less-prominent vertical, southwest trending
3. One less-prominent subhorizontal.

In addition, there are also fractures labeled as randomly oriented that account for a significant portion of all fractures measured in the ESF (CRWMS M&O 1998 [DIRS 102679], p. 37). At Yucca Mountain, the repository is designed with emplacement drift oriented with their axes approximately normal to the southeast trending fracture set. As already discussed in Section 6.2.1, in the Tptpll unit there is also a significant amount of densely spaced small-scale (short tracelength) fractures that connect with lithophysal cavities. The hydraulic significance of these small-scale fractures in relation to the large-scale fractures is unclear. In this study, these small-scale fractures can be considered part of the rock matrix continuum rather than the fracture continuum.

The Tptpmn model domain is a multiple-layered column extending 555.4 m vertically from the top of the tcw13 model layer near the ground surface down to the water table (Table 4.1-3c), with the repository located in the Tptpmn. The vertical layering for the model was chosen to correspond to the vertical contacts at borehole USW SD-9 at about Nevada State Plane Coordinates 171,234 (Easting) and 234,074 (Northing), as implemented in the three-dimensional Yucca Mountain UZ model grid (DTN: LB990501233129.004 [DIRS 111475]) (see Table 4.1.3c for layering dimensions). In the Tptpmn model domain, the emplacement drift is located at an elevation of about 1,065.3 m corresponding to a depth of 220.1 m (1,285.4-1,065.3 = 220.1 m with elevation 1,285.4 extracted from Table 4.1-3c). The elevation 1,065.3 m of the repository corresponds to the location of the repository in UZ model grid (DTN: LB990501233129.004 [DIRS 111475], filename primary.mesh, element 3Ei64, with z-coordinate shown in the rightmost column).

The Tptpll model domain extends 716.6 m vertically from the top of the tcw11 model layer at the ground surface down to the water table (Table 4.1-3d), with the repository located in the Tptpll. The stratigraphy of the Tptpll model domain was taken at a location near the center of the repository at about Nevada State Plane coordinates 170572 m (Easting) and 233195 m (Northing). The geological data are derived from the "j34"column of three-dimensional Yucca Mountain UZ model grid (DTN: LB990501233129.004 [DIRS 111475]) as described in detail in Section 4.1.1.4 (see Table 4.1.3d for layering dimensions). In the Tptpll model domain, the emplacement drift is located at an elevation of about 1082.8 m corresponding to a depth of 363.8 m (1,446.6-1,082.8 = 363.8 m, with elevation 1,446.6 m extracted from Table 4.1-3d). The elevation 1082.8 m of the repository corresponds to the location of the repository in UZ model grid (DTN: LB990501233129.004 [DIRS 111475], filename: primary.mesh, at an average elevation [z = {1085.2863+1080.2863}/2 = 1,082.8 m] of elements 3EJ34 [at z = 1085.2863] and 3FJ34 [at z = 1080.2863], with z-coordinate shown in the rightmost column).

The ground-surface boundary was set at a constant temperature and atmospheric pressure, mechanically free, and the water table boundary was set at a constant temperature and mechanically fixed (Figure 6.3-1 and Table 6.3-1). Specific boundary values used for the Tptpmn model domain represent observations at the locations of the USW SD-9 borehole. The Tptpll model domain uses values representative of the center of the repository at column "j34" of the UZ model grid (DTN: LB9905012331329.004 [DIRS 111475]), as described in detail in Section 4.1.1.4. A varying infiltration rate was applied at the ground surface according to the mean infiltration scenario described in *Simulation of Net Infiltration for Modern and Potential Future Climates* (BSC 2004 [DIRS 170007], Sections 6.9 and 6.11) (Table 6.3-1). The specific infiltration values, 6, 16, and 25 mm/year for the present-day, monsoon, and glacial transition periods, respectively, represent repository-wide averages as calculated in *Drift-Scale Coupled Processes (DST and TH Seepage) Models* (BSC 2004 [DIRS 170338], Appendix B), and presented in DTN: LL000114004242.090 [DIRS 142884] (file: *TSPA_SR_mean_disk1.tar*, chimney_infiltration_fluxes). The mean infiltration scenario is one of three scenarios that represent uncertainties in present-day infiltration and the uncertainty in undisturbed hydrologic properties that arise as a result. The variation of undisturbed hydrological properties does not impact the outcome of this analysis. Thus, for this study, which aims at estimating the impact of any THM-induced disturbance in hydrological properties, it is sufficient to conduct the analysis for the mean-infiltration scenario.

Horizontally, by symmetry, only half of the distance between two adjacent drifts (40.5 m) was modeled because the drift spacing is 81 m. Thus, the left boundary was at the middle plane vertically through a drift, and the right boundary was mid-distance between two adjacent drifts. Both lateral boundaries of the model were mechanically constrained for displacements normal to the boundary and closed for heat and fluid flow by symmetry (Figure 6.3-1). This boundary condition is certainly appropriate for the drifts located in the middle of the repository and for large time after emplacement of the waste compared to the time lag between waste emplacement into two neighboring drifts. The simulation of stress evolution conducted in this

analysis and its comparison to other simulations conducted with mountain-scale models, confirm the appropriateness of the fixed mechanical boundary conditions (Section 6.5.3).

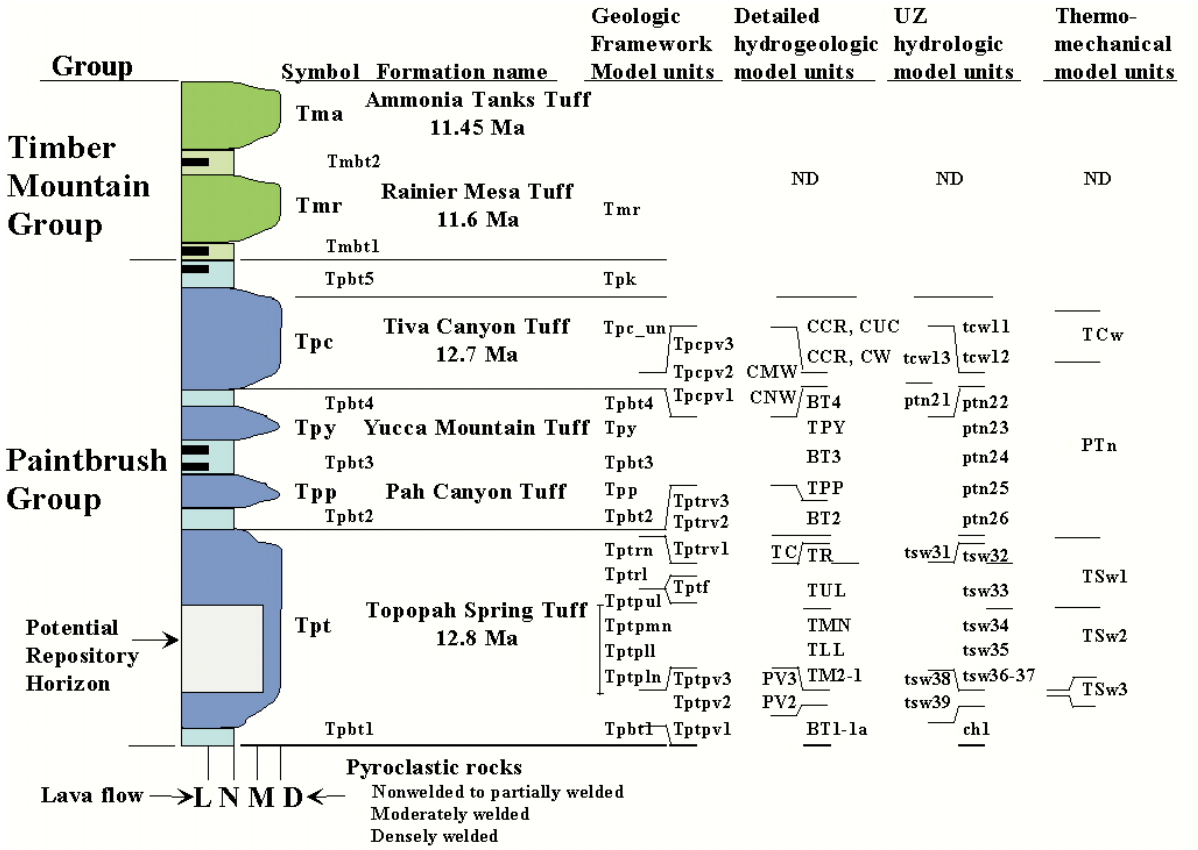

Source: BSC 2004 [DIRS 166107], Figure 6-1.

Figure 6.4-1. Simplified Lithostratigraphic Column of Paintbrush Group and the Rock Units That Form the Repository Horizon

6.4.1 Hydrological and Thermal Properties

The hydrological property set was developed in the mountain-scale calibration runs for the present day ambient conditions at Yucca Mountain (BSC 2004 [DIRS 169857], Section 6.3.2, Table 4). Together with adopted thermal properties, this property set is referred to in this model report as the DS/AFM-UZ02-Mean Property set. It is the same property set considered in both the *Drift-Scale Coupled Processes (DST and TH Seepage) Models* report (BSC 2004 [DIRS 170338], Section 6.2) and *Drift-Scale Coupled Processes (DST and THC Seepage) Models* (BSC 2005 [DIRS 172862], Section 6.5). The properties implicitly account for the effects of lithophysal cavities because they are calibrated against in situ measurements. For an in-depth discussion on the appropriateness of the TH properties, the reader is referred to the *Drift-Scale Coupled Processes (DST and TH Seepage) Models* report (BSC 2004 [DIRS 170338], Section 6.2) and *Calibrated Properties Model* (BSC 2004 [DIRS 169857], Section 6.3.2).

6.4.2 Mechanical Properties

The basic mechanical properties of the rock mass (Young's Modulus and Poisson's ratio) are developed using an established engineering geological rock mass quality classification system

1,000 (an increase by three orders of magnitude), averaging about one order of magnitude (BSC 2004 [DIRS 170004], Section 6.1). It was also found that permeability generally changes more in initially lower-permeability sections.

In this study, the niche excavations were modeled using the FLAC3D V2.0 code to calculate changes in the stress field (Figure 6.4.4-1) using the mechanical properties of the rock mass given in Table 4.1.4. The FLAC3D V2.0 model of the niches is described in Rutqvist (2002 [DIRS 162047], pp. 14 through 18). Based on the calculated stress field, new fracture apertures for each fracture set can be calculated from Equation 6.2-9. The new apertures are then inserted into Equation 6.2-5 to calculate the excavation permeability correction factors F_{kxe}, F_{kye}, and F_{kze} in the x, y, and z direction. Finally, the geometric mean of the excavation permeability correction factors are calculated as:

$$F_{ke} \quad \sqrt[3]{F_{kxe} \times F_{kye} \times F_{kze}} \qquad \text{(Eq. 6.4-6)}$$

As a matching point, a permeability correction factor of $F_{ke} = 9$ is abstracted from *In-Situ Field Testing of Processes* (BSC 2004 [DIRS 170004], Figures 6-19 to 6-23). In these figures, a permeability correction factor of $F_{ke} = 9$ is in good agreement with the observed trend lines for the measured data at Niches 3107, 4788, and CD 1620 at an initial permeability of 1×10^{-13} m^2. A permeability correction factor of $F_{ke} = 9$ represents the mean change in permeability from a large number of measurements taken in 0.3 meter-long borehole intervals. As will be discussed in Section 6.10, it is appropriate to calibrate the model against the mean permeability change in this case because the coupled THM analysis aims at predicting changes in the mean permeability, whereas the permeability distribution remains constant. As shown in Figure 6.10.5-1, the results of the niche-excavation experiments, to which this calibration is made, indicate that the excavation-induced changes in permeability result in a shift in the permeability distribution, while the spread (standard deviation of log permeability) remains approximately constant. Moreover, it is appropriate to calibrate the stress-versus-permeability function against the mean permeability changes caused by the excavation effect because excavation effects are already considered in the seepage analysis (BSC 2004 [DIRS 170338], Section 6.2) as discussed in Section 6.2.4. Thus, the calibrated stress-versus-permeability function provides the best estimate of changes in mean permeability caused by excavation, and a bounding estimate of permeability changes caused by thermally induced stresses.

Figure 6.4.4-2 presents the results of calibrating the parameters b_{max} and α. The two curves in Figure 6.4.4-2 show different combinations of b_{max} and α that satisfy the condition of $F_{kr} = 0.125$ (red curve) and $F_{ke} = 9$ (blue curve). The red curve is determined by a trial-and-error iterative calculation, in which b_{max} is kept fixed at different discrete values between 100 to 400 μm, and for each b_{max}, α is adjusted until the condition $F_{kr} = 0.125$ is satisfied. Similarly, the blue curve is determined by keeping b_{max} fixed and then adjusting α until the condition $F_{ke} = 9$ is satisfied. This calculation, resulting in the red and blue lines of Figure 6.4.4-2, was conducted using an MS Excel spreadsheet as described in Appendix A. A unique solution, satisfying both the condition of $F_{kr} = 0.125$ and $F_{ke} = 9$, is obtained for $b_{max} = 200$ μm and $\alpha = 0.52$ MPa^{-1} (Figure 6.4.4-2). The back-calculated values of $b_{max} = 200$ μm and $\alpha = 0.52$ MPa^{-1} are adopted for all rock units in the drift scale THM model (Section 5, Assumption 6).

Table 6.4.5-1. Summary of TM and HM Parameters and Mechanical Properties of the Rock Mass Developed in This Model Report for the Drift Scale THM Model

Geologic. Unit >		Tptpul	Tptpmn	Tptpll	Source
Initial hydraulic fracture aperture	b_i (μm)	179	77	120	Calculated using Equation 6.4-4 using values of frequency and permeability given in Table 4.1-3a
Maximum joint closure for Equation 6.2-9	b_{max} (μm)	200	200	200	Developed by model calibration against field experiments (Figure 6.4.4-2)
Exponent for α for Equation 6.2-9	α (1/Pa)	5.2E-7	5.2E-7	5.2E-7	Developed by model calibration against field experiments (Figure 6.4.4-2)
Thermal expansion coefficient	α_T (10^{-6}/°C)	5.0+0.0583×T	5.0+0.0583×T	5.0+0.0583×T	Derived from laboratory tests (Figure 6.4.3-1)
Young's Modulus	E (GPa)	19.40	14.77	14.77	Extracted from Excel spreadsheet entitled *THM rock mass modulus v1.xls* (Submitted to TDMS under DTN: LB0306DRSCLTHM.001) in which these properties were derived from the qualified sources listed in Table 4.1-1b under items about intact rock properties and field mapping.
Poisson's Ratio	ν (-)	0.23	0.21	0.21	

T = Temperature in °C.

6.5 SIMULATION RESULTS FOR THE Tptpmn MODEL DOMAIN

This subsection presents modeling results for a representative drift located in the Tptpmn unit. Discussion is focused on permeability changes in the vicinity of the emplacement drift and its impact on the flow field. The impact on the flow field is evaluated by a comparison of fully coupled THM simulation results with partially coupled TH simulation results.

6.5.1 Excavation of the Emplacement Drift

The simulation was conducted by first excavating the drift and then implementing a thermal line load into the drift opening. Excavation of the drift causes stress and permeability changes in the rock mass immediately around the drift (Figures 6.5.1-1a and b). Most changes occur near the top and bottom of the drift, where the horizontal permeability increases by about one order of magnitude. Near the springline of the drift, vertical permeability increases while horizontal permeability decreases, resulting in much smaller changes in mean permeability. The increased permeability at the top of the drift is consistent with measured permeability changes at three excavated niches located in the Tptpmn unit (BSC 2004 [DIRS 170004], Table 6-2).

Figure 6.5.1-1. The maximum correction factor in the Tptpll repository unit (about 8 in Figure 6.6.1-1a) is roughly half of the maximum correction factor in the Tptpmn repository unit (about 19 in Figure 6.5.1-1a). This is explained by the fact that a higher initial permeability and, hence a larger initial fracture aperture in the Tptpll unit, leads to a relatively smaller change in permeability upon excavation. This is also consistent with the general trend of smaller changes in permeability for initially higher permeability values observed at the niche experiments (BSC 2004 [DIRS 170004], Figures 6-19 to 6-23).

The evolution of permeability changes in the Tptpll model domain is presented in Figures 6.6.1-2 and 6.6.1-3. A comparison of these results with corresponding results of permeability correction factors for the Tptpmn model domain in Figures 6.5.4-1 and 6.5.4-2 shows that the general pattern of permeability changes is similar, with early-time permeability changes occurring around the drift, and then gradually spreading away from the drift with time. However, the magnitudes are slightly smaller in the Tptpll model domain than in the Tptpmn model domain. For example, the blue area (F_{kz} < 0.5) extends up to 290 m in the Tptpmn model domain (z = -110 to z = +180 in Figure 6.5.4-1, 1,000 years), but only to about 180 m in the Tptpll model domain (z = +30 to z = +210 in Figure 6.6.1-2, 1,000 years). Furthermore, the minimum permeability correction factor is less than 0.1 in the Tptpmn model domain, whereas in the Tptpll model domain, it is between 0.3 and 0.5. The reason for the relatively smaller changes in permeability in the Tptpll model domain is that the overburden stress is larger, because of the additional geological layers (tcw11-12 and PTn units) on top of the vertical column. The additional geological layers provide about an additional 100 m of overburden, which in turn results in an increased in situ stress at the depth of corresponding geological units. For example, in the Tptpmn model domain, the Tptpmn unit is located at a depth of about 200 m (Table 4.1-3c), whereas in the Tptpll model domain, the Tptpmn unit is located at a depth of about 280 m (Table 4.1-3d). A higher initial stress implies that fractures are more closed, with a higher normal stiffness, and closer to their residual permeability values. All these factors contribute to a relatively smaller change in permeability during the heating of the rock mass.

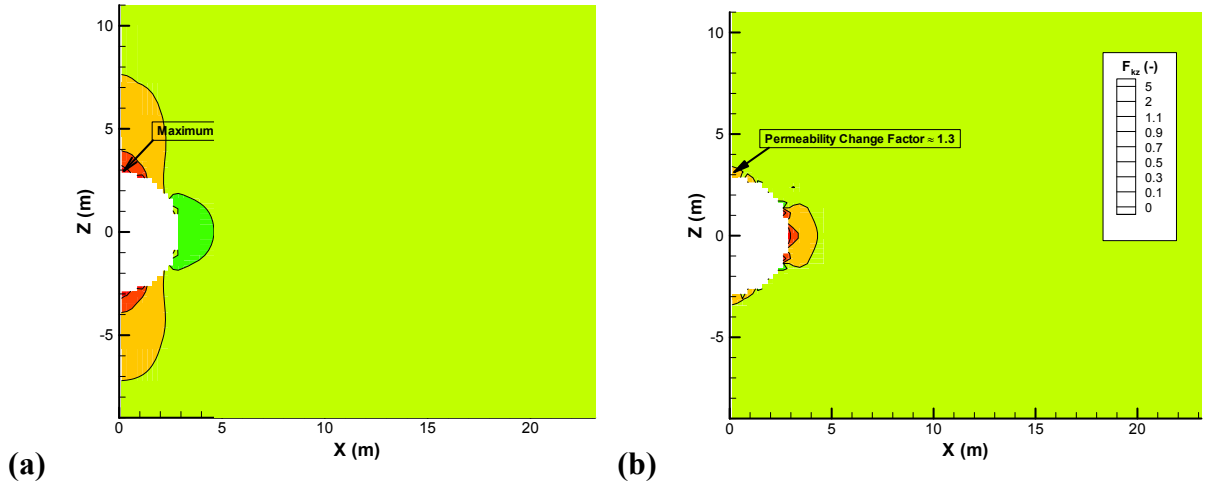

Output DTN: LB0306DRSCLTHM.002.

Figure 6.6.1-1. Permeability Correction Factor Caused by Stress Redistribution During Excavation of the Emplacement Drift: (a) Correction Factor (F_{kx} = k_x/k_i) for Horizontal Permeability, (b) Correction Factor (F_{kz} =k_z/k_i) for Vertical Permeability (Tptpll Model Domain)

possibly occur very close to the drift wall; loose blocks could slip due to a lack of mechanical confinement near the drift wall. Such loosening of blocks and rock fall, which is studied in *Drift Degradation Analysis* (BSC 2004 [DIRS 166107], Sections 6.2 through 6.4), and changes in hydrologic properties for such cases are provided in Section 6.8 of this model report.

6.10.4 Fracture Stress versus Permeability Relationship

The model predictions in this model report depend on the relationship between stress and fracture permeability. The stress-versus-permeability function and the associated stress-versus-aperture function that also determines changes in capillarity were derived as a bounding estimate that emphasizes THM-induced changes in hydrologic properties. The function was calibrated against data from both niche experiments and the DST. The function was calibrated so that it gives the best estimate of mean permeability changes during excavation (for reducing stress), whereas it gives a bounding estimate THM-induced changes in hydrologic properties.

The adopted stress-versus-permeability function gives the best estimate for changes in mean permeability during excavation. As shown in Figure 6.10.5-1, the results of the niche-excavation experiments, to which this calibration is made, indicate that the excavation-induced changes in permeability result in a shift in the permeability distribution, while the spread (standard deviation of log permeability) remains approximately constant. Near the drift wall, the analysis shows that permeability can increase about one order of magnitude in a direction parallel to the drift wall (Figure 6.5.1-1). This magnitude of change is dictated by the fracture normal stress versus permeability function for reducing stress, which both have been calibrated against in situ tests in the Tptpmn and Tptpll units (Figure 6.4.4-1). The fact that mean permeability increases about one order of magnitude near the drift in the Tptpmn unit and less than one order of magnitude in the Tptpll unit is well established from observed permeability changes at excavated niches. *In-Situ Field Testing of Processes* (BSC 2004 [DIRS 170004], Table 6-2) shows that the geometric mean of the post/preratio varies between 9.42 to 25.38 for three niches in the Tptpmn unit; whereas Table 6.1-2-2 shows that the geometric mean of post/preratio is 2.37 for one niche in the Tptpll unit. Thus, the appropriateness of the fracture stress-permeability function to represent excavation effects is established from these field data.

In the longer term, at 1,000 to 10,000 years, the analysis in this model report shows that permeability decreases significantly in an area extending hundreds of meters above and below the drift (Figure 6.5.4-1). The model simulation shows that the permeability decreases most in the vertical direction, by closure of vertical fractures. Such closure of vertical fractures has also been predicted in calculations in *Coupled Thermal-Hydrologic-Mechanical Effects on Permeability Analysis and Models Report* (BSC 2001 [DIRS 155957], Section 7, bullet 2), using the alternative distinct-element model. In this same report (BSC 2001 [DIRS 155957], Section 6.3.3), permeability decreases of up to 6 orders of magnitude were calculated. This was a model artifact having no residual fracture aperture that could limit the amount of fracture closure. Our calculated lower limit of permeability decrease, a factor of 0.03 for vertical permeability in the Tptpmn unit (Figure 6.5.4-3c) and 0.5 in the Tptpll unit (Figure 6.6.1-5b), is strongly dependent on the residual fracture permeability, which was calibrated to field data. This residual permeability is a parameter constrained by the maximum observed decrease in permeability at the DST and SHT. The fact that the parameter is constrained from the maximum

(see also results of niche experiments in Figure 7.5-1). This would indicate that for mechanically-induced increasing permeability (e.g., by unloading near a drift), a larger increase in zones with an initially lower permeability would result in a more homogeneous permeability field. On the other hand, for mechanically induced decreasing permeability (e.g., by thermal stress), the permeability would become more heterogeneous. However, the overall results from the niche experiments show that while the changes in mean permeability are about one order of magnitude, the standard deviation of the heterogeneous permeability field change much less (BSC 2004 [DIRS 170004], Table 6-2). This is further illustrated in Figure 6.10.5-1, which shows the permeability distribution before and after excavation of the niches during the niche experiments. In Figure 6.10.5-1a, which shows the composite excavation response for three niches located in the Tptpmn unit, the excavation induced changes in permeability shift the permeability distribution, while the spread (standard deviation of log permeability) remains approximately constant. Figure 6.10.5-1b, which shows the excavation response for one niche in the Tptpll unit, indicates a smaller shift in relation to its distribution. Figure 6.10.5-1 indicates that the main impact of THM is a change in the mean permeability, even for an initially heterogeneous permeability field. Therefore, it is appropriate to apply the mean permeability changes calculated in this model report to a seepage analysis that considers either the homogenous or heterogeneous permeability field.

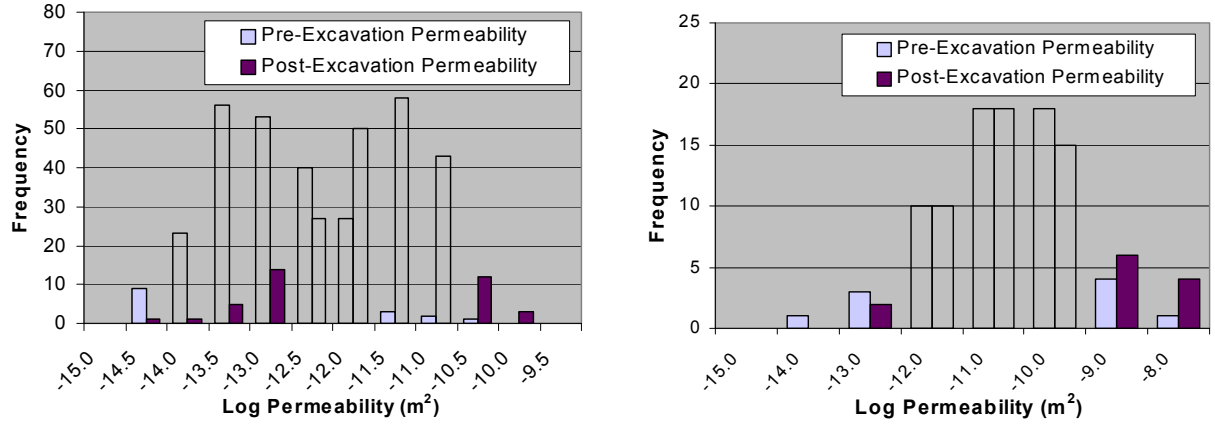

(a) Measurements in Tptpmn unit **(b) Measurements in Tptpll unit**

DTN (measured): LB0310AIRK0015.001 [DIRS 168564]; Output DTN (Histogram plot): LB0306DSTTHMVL.002.

NOTE: Conducted in several boreholes in the crown of three niches (Niche 3107, 3569 and 4788 in the Tptpmn unit, and Niche 1620 in the Tptpll unit).

Figure 6.10.5-1. Histogram of Permeability Distribution Derived from Permeability Measurements

approximate depth of observed underground sidewall damage for Category 1. The model results indicate that the rock adjacent to the drift wall yields in a state of uniaxial compression because the minimum stress at or near the drift wall is zero or small (since the radial stress component is zero). The models also show that, for the range of potential lithophysal rock properties, there is no drift wall yield at the depth of the Tptpul from Category 1. Some of the yield seen in Figure 7.6.3-1 (e.g., for Category 5 above and below the springline) may be caused by the discretization of the circular drift shape, using square elements.

7.6.4 Comparison with Alternative Model of Drift Degradation Analysis

The results of this analysis are consistent with simulation results presented in *Drift Degradation Analysis* (BSC 2004 [DIRS 166107], Section 7.6.5.2), using an alternative modeling approach. In both models, inelastic deformation and yielding take place on the side of the drift and not on the top of the drift. Furthermore, both models predict a yielding of about 0.5 m at the springline (compare Figure 7.6.2-1 in this report with BSC 2004 [DIRS 166107], Section 7.6.5.2, Figures 7-26 and 7-27).

Table 7.6-1. Mechanical Properties Used for Model Validation Against Observations of Sidewall Fracturing in the ECRB Cross Drift

	Category 1	Category 5	Source
Young's Modulus E (GPa)	1.9	19.7	BSC 2004 [DIRS 166107], Appendix E, Table E-10
Bulk Modulus (GPa)	1.07	10.95	BSC 2004 [DIRS 166107], Appendix E, Table E-10
Shear Modulus (GPa)	0.80	8.21	BSC 2004 [DIRS 166107], Appendix E, Table E-10
Cohesion (MPa)	2.33	7.00	BSC 2004 [DIRS 166107], Appendix E, Table E-10
Friction Angle (Degrees)	40	40	BSC 2004 [DIRS 166107], Appendix E, Table E-10
Tensile strength (MPa)	0.8	0.8	DTN: MO0408MWDDDMIO.002 [DIRS 171483], file: *MO0408MWDDDMIO_002RPC1.zip, summary10MPa03seed5.xls*, sheet "envelope-c"

NOTE: Category 1 properties are also listed in Table 4.1-3b for direct input to predictive analysis. The tensile strength of 0.8 was obtained from the x-intercept of the figure in DTN: MO0408MWDDDMIO.002 [DIRS 171483] (file: *MO0408MWDDDMIO_002RPC1.zip*, *summary10MPa03seed5.xls*, sheet "envelope-c"), to be consistent with the drift degradation analysis.

7.7 COMPARISON TO AN ALTERNATIVE CONCEPTUAL MODEL

An additional validation of the drift scale THM model is conducted by comparing this model to the results of a previous analysis of the DST (BSC 2001 [DIRS 155957], Section 6.4.2). In the previous analysis (BSC 2001 [DIRS 155957], Section 6.4.2), the first 18 months of the DST were simulated by two separate three-dimensional analyses, one using a continuum-based model and one using a discrete-fracture model (see Section 1 for a brief description of the alternative discrete-fracture model). In both simulations, the thermal expansion coefficient was set to $9.73°C^{-1}$. In Figure 7.7-1, the simulated results of the previous analysis (BSC 2001

[DIRS 155957], Section 6.4.2) are compared to a separate simulation using the drift scale THM model for displacement at Anchor 4 (located about 15 m from the drift wall) in borehole 148. In this analysis, the drift scale THM model was applied using an equivalent value of the thermal

BSC 2004. *Development of Numerical Grids for UZ Flow and Transport Modeling.* ANL-NBS-HS-000015 REV 02. Las Vegas, Nevada: Bechtel SAIC Company. ACC: DOC.20040901.0001. 169855

BSC 2004. *Drift Degradation Analysis.* ANL-EBS-MD-000027 REV 03. Las Vegas, Nevada: Bechtel SAIC Company. ACC: DOC.20040915.0010. 166107

BSC 2004. *Drift-Scale Coupled Processes (DST and TH Seepage) Models.* MDL-NBS-HS-000015 REV 01. Las Vegas, Nevada: Bechtel SAIC Company. ACC: DOC.20040930.0003. 170338

BSC 2005. *Drift-Scale THC Seepage Model.* MDL-NBS-HS-000001 REV 04. Las Vegas, Nevada: Bechtel SAIC Company. ACC: DOC.20050218.0001. 172862

BSC 2004. *Features, Events, and Processes: Disruptive Events.* ANL-WIS-MD-000005, Rev. 02. Las Vegas, Nevada: Bechtel SAIC Company. 170017

BSC 2004. *Features, Events, and Processes in UZ Flow and Transport.* ANL-NBS-MD-000001, Rev. 03. Las Vegas, Nevada: Bechtel SAIC Company. 170012

BSC 2004. *Geologic Framework Model (GFM2000).* MDL-NBS-GS-000002 REV 02. Las Vegas, Nevada: Bechtel SAIC Company. ACC: DOC.20040827.0008. 170029

BSC 2004. *In Situ Field Testing of Processes.* ANL-NBS-HS-000005, Rev. 03. Las Vegas, Nevada: Bechtel SAIC Company. 170004

BSC 2004. *Mountain-Scale Coupled Processes (TH/THC/THM).* MDL-NBS-HS-000007 REV 02. Las Vegas, Nevada: Bechtel SAIC Company. 169866

BSC 2004. *Q-List.* 000-30R-MGR0-00500-000-000 REV 00. Las Vegas, Nevada: Bechtel SAIC Company. ACC: ENG.20040721.0007. 168361

BSC 2004. *Seepage Model for PA Including Drift Collapse.* MDL-NBS-HS-000002 REV 03. Las Vegas, Nevada: Bechtel SAIC Company. ACC: DOC.20040922.0008. 167652

BSC 2004. *Simulation of Net Infiltration for Present-Day and Potential Future Climates.* MDL-NBS-HS-000023, Rev. 00. Las Vegas, Nevada: Bechtel SAIC Company. 170007

BSC 2004. *Technical Work Plan for: Near-Field Environment and Transport: Near-Field Coupled Processes (TH Seepage and THM) Model Report Integration.* TWP-MGR-PA-000015 REV 00. Las Vegas, Nevada: Bechtel SAIC Company. ACC: DOC.20040610.0001. 170236

BSC 2004. *Technical Work Plan for: Performance Assessment Unsaturated Zone.* TWP-NBS-HS-000003 REV 02 Errata 001. Las Vegas, Nevada: Bechtel SAIC Company. ACC: MOL.20030102.0108; DOC.20040121.0001. 167969